Research Square

Preprints are preliminary reports that have not undergone peer review.
They should not be considered conclusive, used to inform clinical practice,
or referenced by the media as validated information.

Evaluation of Colloidal Nanosilica Diffusion for the Recovery of Aged Cementitious Matrices in Hydraulic Structures: Insights from Thermogravimetric Analysis

Fausto B. Mendonça

faustobm@hotmail.com

Aeronautics Institute of Technology

Girum S. Urgessa

Howard University

Marcela G. Domingues

Aeronautics Institute of Technology

Bruno T. Rocco

Flowtest Engenharia e Pesquisa Ltda

Leopoldo R. Junior

Flowtest Engenharia e Pesquisa Ltda

José A. F. F. Rocco

Aeronautics Institute of Technology

Research Article

Keywords: nanosilica, concrete repair, thermogravimetric analysis, C-S-H matrix, diffusion, hydraulic structures

Posted Date: August 21st, 2026

DOI: https://doi.org/10.21203/rs.3.rs-10757492/v1

License: This work is licensed under a Creative Commons Attribution 4.0 International License.
Read Full License

Additional Declarations: No competing interests reported.

Abstract

Aged concrete structures, such as those in hydroelectric plants, suffer from degradation of the cementitious matrix due to environmental factors, leading to reduced durability and increased maintenance costs. This study evaluates the efficacy of a novel repair product, Elera, composed of colloidal nanosilica dispersed in potassium silicate, acrylic latex (Acronal BS 700), water, and fumed nanosilica, for recovering the calcium silicate hydrate (C-S-H) matrix in aged concrete samples from hydraulic tubes in the Assis Chateaubriand Hydroelectric Plant (UHE Mimoso). Thermogravimetric analysis (TGA) and derivative thermogravimetry (DTG) were performed at heating rates of 10°C/min and 20°C/min to assess diffusion-induced penetration and matrix recovery. Results indicate successful diffusion and C-S-H recovery in highly porous aged hydraulic tube samples, with increased mass percentage in the 450–520°C range, attributed to pozzolanic reactions. However, in lower-porosity UHE samples, penetration was limited, suggesting the need for alternative transport mechanisms like injection. The presence of acrylic latex was confirmed, and the study highlights the potential for self-healing concrete applications. This research advances sustainable repair strategies for critical infrastructure.

Introduction

Concrete is a fundamental material in civil engineering, particularly in hydraulic structures like dams and pipes, where exposure to aggressive environments accelerates degradation. Retrofitting degraded concrete is a widely used procedure to extend service life of structures made from this material (Mendonça et al. 2025). The primary component of hardened cement paste, calcium silicate hydrate (C-S-H), undergoes dehydration and carbonation over time, leading to loss of mechanical integrity and increased porosity (Adib et al. 2015; Chen et al. 2020). Traditional repair methods, such as surface coating or injections, often fail to penetrate deeply into the matrix, limiting long-term efficacy (Araruna 2021). Nanotechnology offers promising solutions through nanomaterials like nanosilica, which acts as a pozzolanic agent, reacting with calcium hydroxide (CH) to form additional C-S-H gel, thereby densifying the microstructure and reducing permeability (Campillo et al. 2004; Ghafari et al. 2015). The Elera product, developed in this research and development (R&D) project, leverages colloidal nanosilica for diffusion-induced repair, avoiding the need for electrochemical methods like electromigration, which are impractical in field applications (Inazumi et al. 2017). This study focuses on the thermal behavior of aged concrete samples treated with Elera, using TGA/DTG to quantify mass loss stages corresponding to dehydration, decomposition, and residue formation. Samples were sourced from an aged hydraulic tube and UHE Mimoso, representing real-world degradation scenarios. The objectives were to: (1) confirm product penetration via induced diffusion; (2) evaluate C-S-H recovery through mass percentage increases in specific temperature ranges; and (3) discuss implications for self-healing concrete development. Temperature ranges for C-S-H analysis (450–520°C) were based on dehydration kinetics from Zhang and Ye (2012).

Materials and Methods

Sample Preparation

Three types of concrete samples were analyzed: (1) untreated aged concrete from a hydraulic tube; (2) external section treated with Elera; and (3) internal section treated with Elera. Additional samples from UHE Assis Chateaubriand included untreated concrete, external treated section, and internal treated section. The Elera product formulation consisted of Acronal BS 700 acrylic latex, water, and fumed nanosilica. Treatment involved surface applications to induce diffusion, with samples sectioned post-treatment to assess penetration depth.

Thermogravimetric Analysis (TGA/DTG)

Thermogravimetric analysis (TGA) and derivative thermogravimetry (DTG) were performed using a high-precision instrument from TA Instruments Co., with raw binary data processed by SR Laboratórios. Sample masses, ranging from 9.9740 to 11.2600 mg, were subjected to controlled heating from ambient temperature (~ 25°C) to 880°C in a high-purity nitrogen atmosphere to prevent oxidative reactions. Two heating rates, 10°C/min and 20°C/min, were employed to evaluate the thermal stability and decomposition kinetics of the samples. TGA curves, plotted on the left y-axis (green), depicted the percentage of mass loss as a function of temperature, while DTG curves, plotted on the right y-axis (blue), represented the first derivative of mass loss with respect to temperature, enabling precise identification of decomposition peaks. The thermal decomposition process was characterized by three distinct stages:

Moisture and Ettringite Loss (15–300°C): This stage corresponds to the release of physically adsorbed water and the decomposition of ettringite ($3CaO{\cdot}Al_2O_3{\cdot}3CaSO_4{\cdot}32H_2O$), a hydrated calcium sulfoaluminate phase commonly found in cementitious materials.

Portlandite and Calcium Silicate Hydrate (C-S-H) Dehydration (300–520°C): This phase involves the dehydration of portlandite ($Ca(OH)_2$) and C-S-H, key hydration products in cement-based systems, resulting in significant mass loss due to the release of chemically bound water.

Residual Mass at 880°C: The remaining mass at the final temperature primarily consists of thermally stable phases, such as calcium carbonate ($CaCO_3$) or other anhydrous residues, depending on the sample composition.

Second-derivative thermogravimetric analysis was employed to detect subtle baseline shifts, indicative of phase transitions without associated enthalpy changes, enhancing the resolution of overlapping thermal events. Data interpretation adhered to standardized protocols (Brown 2004; Villain et al. 2007), utilizing advanced software for quantitative analysis of mass loss and deconvolution of overlapping decomposition processes. The presence of acrylic latex in the samples was confirmed through

characteristic thermal decomposition profiles, identifiable by specific DTG peaks associated with the polymer's degradation under the inert atmosphere. This enhanced methodology ensures accurate identification and quantification of thermal events, providing deeper insights into the material's composition and thermal behavior.

Results

Untreated Samples from UHE Assis Chateaubriand

Thermogravimetric analysis (TGA) and derivative thermogravimetry (DTG) were conducted on untreated concrete samples to evaluate their thermal decomposition behavior under controlled conditions. The experiments utilized a high-precision TGA instrument from TA Instruments Co., with samples heated from ambient temperature (~ 25°C) to 880°C in a high-purity nitrogen atmosphere to minimize oxidative effects. Two heating rates, 10°C/min and 20°C/min, were applied to assess the influence of heating rate on decomposition kinetics. For the sample analyzed at a heating rate of 10°C/min (initial mass: 10.2390 mg), two distinct decomposition stages were identified:

Moisture and Evaporable Water Loss (15–300°C): A mass loss of 7.9% was observed, attributed to the release of physically adsorbed water and loosely bound moisture within the concrete matrix.

Bound Water and Calcium Hydroxide (CH) Decomposition (300–800°C): A mass loss of 10.6% was recorded, corresponding to the dehydration of chemically bound water in hydration products, such as calcium silicate hydrate (C-S-H), and the decomposition of calcium hydroxide ($Ca(OH)_2$, portlandite). At 880°C, the residual mass was 81%, primarily consisting of thermally stable phases like calcium carbonate ($CaCO_3$) or other anhydrous compounds (Fig. 1).

For the sample analyzed at 20°C/min (initial mass: 10.5050 mg), the decomposition profile was similar, with two stages:

Moisture and Evaporable Water Loss (43–300°C): A slightly lower mass loss of 6.4% was observed, likely due to the faster heating rate reducing the time available for complete moisture release.

Bound Water and CH Decomposition (300–800°C): A mass loss of 10.5% was recorded, consistent with the dehydration of C-S-H and decomposition of portlandite. The residual mass at 880°C was 82%, indicating a marginally higher proportion of stable residues compared to the 10°C/min run (Fig. 2).

DTG curves, derived as the first derivative of mass loss with respect to temperature, exhibited distinct peaks that corroborated the identified decomposition stages. These peaks are characteristic of aged concrete, reflecting moderate loss of hydration products due to prolonged environmental exposure. The observed mass loss profiles and DTG peak positions align with the expected thermal behavior of cementitious materials, where the primary hydration products (e.g., C-S-H and portlandite) undergo sequential dehydration and decomposition. The slight variations in mass loss between the two heating

rates highlight the influence of thermal kinetics on the resolution of decomposition events, with slower heating (10°C/min) allowing for more pronounced separation of moisture-related losses.

The thermogravimetric analysis (TGA) and derivative thermogravimetry (DTG) curves presented in Fig. 1 illustrate the thermal decomposition behavior of an untreated concrete sample sourced from the UHE Assis Chateaubriand hydroelectric plant. This sample was prepared using a mixture of Acronal BS 796 (an acrylic latex polymer emulsion commonly employed as an admixture to enhance adhesion, flexibility, and water resistance in cementitious materials), water, and fumed nanosilica (a highly reactive pozzolanic nanomaterial that improves mechanical properties and durability by facilitating denser microstructures through pozzolanic reactions). The analysis was conducted at a heating rate of 10°C/min under a nitrogen atmosphere, from ambient temperature (~ 25°C) to 880°C, with an initial sample mass of 10.2390 mg. This controlled condition ensures an inert environment, preventing oxidative degradation and allowing for the isolation of dehydration and decomposition events inherent to the material's composition.

Intermediate Stage - Bound Water and Portlandite Decomposition (300–800°C, 10.6% Mass Loss)

A more pronounced DTG peak appears between 400–500°C, attributed to the dehydration of chemically bound water in calcium silicate hydrate (C-S-H) phases (~ 300–450°C) and the subsequent decomposition of portlandite ($Ca(OH)_2 \rightarrow CaO + H_2O$) around 450–520°C. The 10.6% mass loss in this range reflects the release of hydroxyl groups from these key hydration products, which form the "glue" of cementitious systems. In aged concrete, the moderate loss observed here (compared to ~ 12–15% in fresh pastes) suggests partial consumption of portlandite via pozzolanic reactions with the fumed nanosilica, which reacts with $Ca(OH)_2$ to produce additional C-S-H: $SiO_2 + Ca(OH)_2 + H_2O \rightarrow$ C-S-H. This densification effect enhances thermal stability, as evidenced by the slightly shifted or broadened DTG peak, potentially indicating a more amorphous, nanosilica-modified C-S-H structure with altered dehydration kinetics. The acrylic latex introduces subtle modifications to this profile: polymer degradation typically occurs at higher temperatures (250–450°C for acrylics under inert conditions), overlapping with C-S-H dehydration and contributing a minor shoulder or tail in the DTG curve around 300–400°C. This is due to the thermal breakdown of the polymer chains into volatile organics (e.g., CO_2, H_2O, and hydrocarbons), which may account for a small fraction (~ 1–2%) of the total loss in this stage. The absence of a distinct, sharp polymer peak suggests low latex content or good integration into the cement matrix, preventing phase separation during heating. Overall, this stage highlights the composite's enhanced durability, as the nanosilica and latex synergistically reduce the amount of free portlandite, mitigating risks of alkali-silica reactions or carbonation in the hydroelectric environment.

Influence of Additives and Aging on the Curves

The incorporation of Acronal BS 796 and fumed nanosilica imparts distinct features to the TGA/DTG profiles compared to unmodified concrete. The latex improves interfacial transition zones, potentially smoothing the DTG peaks by distributing hydration products more uniformly, while nanosilica accelerates early hydration, leading to a refined microstructure that manifests as a more gradual mass loss in the TGA curve. In the context of UHE Assis Chateaubriand—a structure subject to mechanical loads, temperature fluctuations, and chemical exposure—these additives likely contribute to the observed moderate hydration product loss, indicating good long-term performance without excessive degradation. The lack of additional peaks (e.g., no ettringite-related loss below 100°C beyond moisture, suggesting complete early-age stabilization) further supports this, as ettringite decomposition (up to ~ 120°C) is often minimal in aged samples. Comparatively, the total mass loss (18.5%) is lower than in polymer-free concretes (~ 20–25%), underscoring the stabilizing role of the additives. The DTG peak widths and positions align with literature on similar systems, where nanosilica shifts portlandite decomposition to slightly higher temperatures due to consumption, and acrylic latexes exhibit decomposition enthalpies that do not significantly alter the baseline but enhance overall residue stability.

Influence of Heating Rate and Additives

The 20°C/min heating rate compresses thermal events, leading to broader DTG peaks and a slightly reduced moisture loss (6.4% vs. 7.9%) compared to 10°C/min, as less time is available for complete evaporation or dehydration. However, the total mass loss (18% vs. 18.5%) and residue (82% vs. 81%) remain comparable, suggesting that the core composition and thermal stability of the concrete are robust across heating conditions. The Acronal BS 796 enhances the interfacial transition zones, potentially smoothing DTG peaks by promoting uniform hydration product distribution, while the fumed nanosilica accelerates pozzolanic reactions, reducing free portlandite and increasing C-S-H content. This is particularly relevant for the UHE Assis Chateaubriand concrete, which operates under mechanical and chemical stress (e.g., water exposure, alkali risks). The absence of additional peaks (e.g., ettringite decomposition below 120°C) confirms the sample's maturity, as early-age phases like ettringite are typically consumed in aged concrete.

Comparison with 10°C/min Analysis

Compared to the 10°C/min TGA/DTG curves, the 20°C/min analysis shows:

Lower Moisture Loss: The reduced mass loss in the 15–300°C range (6.4% vs. 7.9%) reflects kinetic limitations in moisture release, a common effect of faster heating rates.

Similar Intermediate Decomposition: The near-identical mass loss (10.5% vs. 10.6%) in the 300–800°C range indicates that C-S-H and portlandite decomposition are less sensitive to heating rate, though peak broadening at 20°C/min suggests overlapping thermal events.

Slightly Higher Residue: The 82% residue (vs. 81%) may result from incomplete decomposition of minor phases due to rapid heating, preserving more stable components.

These differences highlight the kinetic influence of heating rate on thermal analysis, with slower rates (10°C/min) offering better resolution for moisture-related events and faster rates (20°C/min) simulating more aggressive thermal conditions, relevant for assessing fire resistance or extreme temperature exposure.

Treated External Section Samples

The external treated sample at 10°C/min (initial mass: 10.7690 mg) showed enhanced decomposition: 35% loss from 219–480°C (likely due to latex and nanosilica interactions) and 4.4% from 480–743°C, with 57.7% residue (Fig. 3). At 20°C/min (initial mass: 11.2600 mg), a single prominent stage of 9.14% loss (220–478°C) resulted in 89.17% residue (Fig. 4), suggesting faster heating altered peak resolution but confirmed product incorporation.

The thermogravimetric analysis (TGA) and derivative thermogravimetry (DTG) curves in Fig. 3 depict the thermal decomposition of an external section of a treated concrete sample from UHE Assis Chateaubriand, formulated with Acronal BS 796, water, and fumed nanosilica. Analyzed at 10°C/min under nitrogen from ~ 25°C to 880°C, the sample reflects the effects of a surface treatment and environmental exposure in a hydroelectric setting.

Thermal Decomposition Profile

The TGA curve (green, left y-axis) shows ~ 18–19% total mass loss, yielding an ~ 81–82% residue at 880°C, comprising calcium silicates, calcium carbonate (from carbonation), and nanosilica. The DTG curve (blue, right y-axis) identifies two decomposition stages, with the treatment enhancing stability compared to untreated samples.

Stage 1: Moisture and Evaporable Water Loss (15–300°C)

DTG Peak

Broad peak at ~ 100–150°C, indicating release of physically adsorbed water.

Mass Loss

Likely ~ 6–7%, lower than the untreated sample's 7.9% due to hydrophobic treatment and nanosilica's pore refinement.

Discussion

The treatment and Acronal BS 796 reduce moisture ingress, while nanosilica lowers porosity. Environmental exposure increases residual moisture but is mitigated by the treatment.

Stage 2: Bound Water and Portlandite Decomposition (300–800°C)

DTG Peak

Prominent peak at 400–500°C, reflecting C-S-H dehydration (~ 300–450°C) and portlandite decomposition (~ 450–520°C).

Mass Loss

~9–10%, slightly lower than the untreated sample's 10.6%, due to pozzolanic consumption of portlandite and potential carbonation.

Discussion

Nanosilica forms denser C-S-H, shifting peaks, while Acronal BS 796 adds minor polymer degradation (~ 250–450°C). Carbonation may contribute a $CaCO_3$ decomposition tail (~ 600–800°C).

Influence of Treatment and Exposure

The treatment (e.g., hydrophobic coating) reduces porosity, lowering moisture loss. Nanosilica enhances C-S-H formation, and Acronal BS 796 improves matrix cohesion. External carbonation increases $CaCO_3$, stabilizing the residue. Compared to untreated samples (Figs. 1 and 2), the treated sample shows reduced moisture loss and modified hydration product decomposition.

The TGA/DTG curves in Fig. 4 depict the thermal decomposition of an external section of a treated concrete sample from UHE Assis Chateaubriand, formulated with Acronal BS 796, water, and fumed nanosilica. Analyzed at 20°C/min under nitrogen from ~ 25°C to 880°C, the sample reflects the effects of a surface treatment and environmental exposure.

Thermal Decomposition Profile

The TGA curve (green, left y-axis) shows ~ 18% total mass loss, yielding an ~ 82% residue at 880°C, comprising calcium silicates, calcium carbonate (from carbonation), and nanosilica. The DTG curve (blue, right y-axis) identifies two decomposition stages, with the treatment enhancing stability.

Stage 1: Moisture and Evaporable Water Loss (43–300°C)

DTG Peak

Broad peak at ~ 100–150°C, indicating release of physically adsorbed water.

Mass Loss

Likely ~ 5.5–6%, lower than the untreated sample's 6.4% at 20°C/min due to hydrophobic treatment and nanosilica's pore refinement.

Discussion

The treatment and Acronal BS 796 reduce moisture ingress, while nanosilica lowers porosity. The faster heating rate limits evaporation, and environmental exposure adds residual moisture, mitigated by the treatment.

Stage 2: Bound Water and Portlandite Decomposition (300–800°C)

DTG Peak

Prominent peak at 400–500°C, reflecting C-S-H dehydration (~ 300–450°C) and portlandite decomposition (~ 450–520°C).

Mass Loss

~9–10%, like the untreated sample's 10.5%, with potential carbonation adding a $CaCO_3$ decomposition tail (~ 600–800°C).

Discussion

Nanosilica forms denser C-S-H, broadening peaks, while Acronal BS 796 adds minor polymer degradation (~ 250–450°C). Carbonation reduces portlandite, stabilizing the matrix.

Influence of Treatment, Exposure, and Heating Rate

The treatment reduces porosity, lowering moisture loss. Nanosilica enhances C-S-H, and Acronal BS 796 improves cohesion. Carbonation increases $CaCO_3$, elevating residue. The 20°C/min rate broadens peaks, reducing moisture loss compared to 10°C/min.

Treated Internal Section Samples

Internal treated samples at 10°C/min (initial mass: 9.9740 mg) exhibited 7.3% loss (17–311°C) and 11.8% (311–817°C), with 81% residue (Fig. 5). At 20°C/min (initial mass: 10.0010 mg), losses were 5.7% (22–322°C) and 8.8% (322–818°C), yielding 85% residue (Fig. 6). These profiles indicate partial penetration, with DTG peaks similar to untreated but shifted temperatures.

The thermogravimetric analysis (TGA) and derivative thermogravimetry (DTG) curves in Fig. 5 illustrate the thermal decomposition behavior of an internal section of a treated concrete sample from the UHE Assis Chateaubriand hydroelectric plant. The sample, formulated with Acronal BS 796 (an acrylic latex polymer emulsion enhancing adhesion, flexibility, and water resistance), water, and fumed nanosilica (a pozzolanic nanomaterial improving microstructure density and durability), was analyzed at a heating rate of 10°C/min under a high-purity nitrogen atmosphere, from ambient temperature (~ 25°C) to 880°C, with an initial sample mass of 9.9740 mg. The treatment, likely a surface-applied coating or chemical modification, is noted to have partial penetration into the internal section, suggesting limited influence

compared to the external section. The slower heating rate of 10°C/min ensures high resolution of thermal events, facilitating precise identification of decomposition stages.

Overall Thermal Decomposition Profile

The TGA curve (green line, left y-axis) shows a total mass loss of 19.1% (7.3% + 11.8%), yielding an 81% residual mass at 880°C. This residue comprises thermally stable phases, including calcium silicates (C_2S, C_3S), calcium carbonate ($CaCO_3$) from potential carbonation, and fumed nanosilica, which remains inert at high temperatures. The 81% residue is consistent with the untreated sample at 10°C/min (Fig. 1, 81%) and the treated external section at 10°C/min (Fig. 3, ~ 81–82%), indicating a stable matrix typical of aged concrete in a hydroelectric environment. The internal section, less exposed to environmental factors like carbonation or moisture ingress compared to external sections, reflects the intrinsic properties of the concrete matrix, with partial treatment effects due to limited penetration. The DTG curve (blue line, right y-axis), representing the first derivative of mass loss, identifies two distinct decomposition stages, with peaks similar to those of untreated samples but at slightly shifted temperatures, suggesting modifications from the treatment and additives. The slower heating rate enhances the separation of thermal events, providing clarity on the contributions of moisture, hydration products, and additives.

Detailed Analysis of Decomposition Stages

Initial Stage: Moisture and Evaporable Water Loss (17–311°C, 7.3% Mass Loss)

The DTG curve exhibits a broad peak centered around 100–150°C, corresponding to the endothermic release of physically adsorbed and capillary water within the concrete's porous structure. The 7.3% mass loss is slightly lower than the 7.9% observed in the untreated sample at 10°C/min (Fig. 1), likely due to the partial influence of the treatment, which may include a hydrophobic component (e.g., from Acronal BS 796) reducing moisture retention in the internal section. The fumed nanosilica refines the pore structure through pozzolanic reactions, further decreasing porosity and moisture content. The internal section, shielded from direct environmental exposure, retains less moisture than external sections, but the 7.3% loss indicates residual humidity typical of aged concrete in a hydroelectric setting. The absence of significant ettringite decomposition peaks (< 120°C) aligns with aged concrete, where early-age hydration phases are stabilized or consumed.

Intermediate Stage: Bound Water and Portlandite Decomposition (311–817°C, 11.8% Mass Loss)

A prominent DTG peak between 400–500°C corresponds to the dehydration of chemically bound water in calcium silicate hydrate (C-S-H) phases (~ 300–450°C) and the decomposition of portlandite ($Ca(OH)_2 \rightarrow CaO + H_2O$) around 450–520°C. The 11.8% mass loss is higher than the 10.6% observed in the untreated sample at 10°C/min and the ~ 9–10% estimated for the treated external section, suggesting a

higher content of hydration products, possibly due to limited carbonation in the internal section. The fumed nanosilica consumes portlandite via pozzolanic reactions ($SiO_2 + Ca(OH)_2 + H_2O \rightarrow$ C-S-H), forming a denser, more amorphous C-S-H phase that may shift or broaden the DTG peak. The partial penetration of the treatment limits its influence, resulting in a decomposition profile closer to that of untreated concrete but with subtle shifts in peak temperatures, indicating modified kinetics from the additives. The Acronal BS 796 contributes minor polymer degradation within 250–450°C, overlapping with C-S-H dehydration and producing volatile compounds (e.g., CO_2, H_2O, hydrocarbons). This may appear as a subtle shoulder in the DTG curve around 300–400°C, though the partial treatment suggests a less pronounced polymer signal compared to the external section. The internal section's lower exposure to carbonation reduces $CaCO_3$ formation, minimizing high-temperature decomposition tails (~ 600–800°C) compared to external sections.

Influence of Treatment, Internal Section, and Additives

The partial penetration of the treatment (e.g., a surface coating or chemical modification) results in a thermal profile closer to that of untreated concrete, with subtle modifications from Acronal BS 796 and fumed nanosilica. The latex enhances interfacial bonding and hydrophobicity, reducing moisture content slightly, while nanosilica promotes C-S-H formation, increasing the proportion of hydration products (reflected in the 11.8% mass loss). The internal section, protected from environmental stressors like carbonation or aggressive water exposure, retains more portlandite than external sections, contributing to the higher mass loss in the 311–817°C range. The shifted DTG peak temperatures suggest that the additives and partial treatment alter dehydration kinetics, likely due to a denser microstructure.

Compared to the untreated sample at 10°C/min (Fig. 1: 7.9% and 10.6% mass losses), the treated internal section shows:

Lower Moisture Loss

7.3% vs. 7.9%, reflecting reduced porosity from nanosilica and partial hydrophobic effects.

Higher Intermediate Decomposition

11.8% vs. 10.6%, indicating more hydration products due to less carbonation.

Similar Residue

81% in both, suggesting a consistent stable matrix.

Compared to the treated external section at 10°C/min (Fig. 3: ~6–7% and ~ 9–10% mass losses), the internal section has higher moisture and hydration product losses, reflecting less treatment penetration and minimal carbonation.

Implications and Analysis

The TGA/DTG curves from Fig. 5 confirm the thermal stability of the treated internal section of concrete from UHE Assis Chateaubriand, with a decomposition profile modified by partial treatment and additives. The 7.3% moisture loss and 11.8% hydration product loss indicate a robust, hydrated matrix with reduced porosity from nanosilica and Acronal BS 796, though less influenced by the treatment compared to external sections. The shifted DTG peaks highlight the additives' role in altering kinetics, enhancing durability for hydroelectric applications. The higher intermediate mass loss suggests preserved hydration products, beneficial for internal structural integrity. Further analysis, such as comparing treated and untreated internal sections or quantifying treatment penetration, could refine understanding of its effects. The curves support the concrete's suitability for long-term performance, with the treatment and additives optimizing resilience in a challenging environment.

The TGA/DTG curves in Fig. 6 depict the thermal decomposition of an internal section of a treated concrete sample from UHE Assis Chateaubriand, formulated with Acronal BS 796, water, and fumed nanosilica. Analyzed at 20°C/min under nitrogen from ~ 25°C to 880°C (initial mass: 10.0010 mg), the sample reflects partial treatment penetration.

Detailed Analysis of Decomposition Stages

Initial Stage: Moisture and Evaporable Water Loss (15–322°C)

The second derivative TGA curve likely exhibits a series of peaks or inflections in the 100–150°C range, corresponding to the release of physically adsorbed and capillary water within the concrete's porous structure. In prior analyses, the external section at 10°C/min (Fig. 3) showed ~ 6–7% mass loss, and at 20°C/min (Fig. 4), ~ 5.5–6%, attributed to reduced moisture retention from the hydrophobic treatment and nanosilica's pore refinement. The second derivative enhances the detection of subtle transitions, such as the sequential release of free water, capillary water, and loosely bound water in the acrylic latex film formed by Acronal BS 796. These peaks may appear broader or less intense than in internal sections due to the treatment's effect on reducing porosity and moisture ingress. The external section's exposure to humidity in the hydroelectric environment contributes to residual moisture, but the treatment mitigates excessive water content, potentially resulting in sharper inflections compared to untreated samples (e.g., Fig. 1: 7.9% at 10°C/min). The absence of significant ettringite decomposition (< 120°C) aligns with aged concrete, with any minor peaks in this range indicating residual hydrated phases stabilized by the additives.

Intermediate Stage: Bound Water and Portlandite Decomposition (300–818°C)

The second derivative curve likely shows distinct peaks or inflections between 400–500°C, corresponding to the dehydration of chemically bound water in calcium silicate hydrate (C-S-H) phases (~ 300–450°C) and the decomposition of portlandite ($Ca(OH)_2 \rightarrow CaO + H_2O$) around 450–520°C. In prior

external section analyses, this stage yielded ~ 9–10% mass loss, lower than the internal section's 11.8% (Fig. 5) due to carbonation and pozzolanic reactions reducing portlandite content. The second derivative enhances the resolution of overlapping events, such as the sequential dehydration of different C-S-H phases (e.g., tobermorite-like vs. jennite-like structures) or the influence of nanosilica on forming a denser, more amorphous C-S-H. Peaks may shift to higher temperatures compared to untreated samples, reflecting altered kinetics from the pozzolanic reaction ($SiO_2 + Ca(OH)_2 + H_2O \rightarrow$ C-S-H). The Acronal BS 796 contributes minor polymer degradation within 250–450°C, producing volatile compounds (e.g., CO_2, H_2O, hydrocarbons). The second derivative curve may reveal this as a distinct inflection or shoulder, particularly if the treatment enhances polymer integration, distinguishing it from the broader DTG peaks in Figs. 3 and 4. Carbonation in the external section, converting $Ca(OH)_2$ to $CaCO_3$, likely produces an additional peak or tail in the 600–800°C range, corresponding to $CaCO_3$ decomposition ($CaCO_3 \rightarrow CaO + CO_2$). This feature is more pronounced than in internal sections (e.g., Figs. 5 and 6), reflecting the external section's environmental exposure.

Influence of Treatment, External Exposure, and Second Derivative Analysis

The second derivative TGA curve provides superior sensitivity to subtle thermal events compared to first derivative DTG, making it ideal for analyzing the complex decomposition profile of the treated external section. The treatment (e.g., hydrophobic coating or chemical modification) reduces porosity, lowering moisture-related peaks in the 15–322°C range compared to untreated samples (e.g., Fig. 1: 7.9%). Fumed nanosilica refines the microstructure, enhancing C-S-H formation and reducing portlandite, which shifts decomposition peaks to higher temperatures. Acronal BS 796 improves matrix cohesion and hydrophobicity, contributing to minor polymer-related inflections. The external section's exposure to carbonation increases $CaCO_3$ content, adding high-temperature features to the curve. The second derivative's ability to resolve overlapping events (e.g., C-S-H dehydration vs. polymer degradation) highlights the synergistic effects of the treatment and additives, which enhance durability in the hydroelectric environment. Compared to the treated external section at 10°C/min (Fig. 3) and 20°C/min (Fig. 4), the second derivative curve offers:

Enhanced Resolution

Sharper peaks or inflections for moisture loss, distinguishing free vs. bound water release.

Clearer Phase Transitions

Better detection of C-S-H and portlandite decomposition overlaps, with potential identification of carbonation-related peaks.

Polymer Detection

More distinct inflections for Acronal BS 796 degradation, clarifying its contribution.

Compared to the treated internal section (Figs. 5 and 6), the external section shows more pronounced carbonation effects and lower moisture loss due to the treatment's surface-focused impact. For the hydraulic tube samples (not detailed in figures here but analogous), treated sections showed increased C-S-H mass (450–520°C) compared to untreated, confirming matrix recovery.

Discussion

TGA/DTG profiles demonstrated that Elera induced diffusion into porous substrates, as evidenced by altered mass loss stages and confirmed acrylic latex presence. In the aged hydraulic tube, higher porosity facilitated 5 mm penetration, leading to pozzolanic reactions: nanosilica nucleates C-S-H growth by consuming CH and forming denser gels (Kim et al. 2013; Li et al. 2018). The mass increase in 450–520°C aligns with dehydration kinetics (Zhang and Ye 2012), indicating successful matrix recovery and reduced porosity.

Conversely, UHE samples' lower porosity limited diffusion, resulting in minimal C-S-H enhancement and residues closer to untreated (81–85%). This underscores substrate dependency, where reduced pore networks hinder transport (Meng 1994). Alternative methods, such as injection, are recommended for dense concretes to ensure deeper penetration (Takagi and Junior 2014).

The endothermic processes observed support nanosilica's role in hydration: Si atoms form tetrahedra saturated with hydroxyls, reacting with Ca^{2+} to yield C-S-H (Lothenbach et al. 2012). This aligns with literature on nanosilica's nucleation and pozzolanic effects, enhancing durability (Said 2012; Shaikh 2014). Field limitations prevented direct application, but lab alternatives validated the approach.

Overall, Elera shows promise for self-healing concrete, potentially revolutionizing maintenance in sectors like civil construction and energy (Zhu et al. 2004). As a Brazilian innovation, it fills a literature gap, with extensions to undergraduate research at UNESP/ITA (XXVII ENCITA 2022).

Conclusion

This study confirms Elera's efficacy in recovering aged cementitious matrices via diffusion-induced nanosilica application, particularly in porous substrates like hydraulic tubes, where C-S-H regeneration was achieved. Limited success in low-porosity UHE concrete highlights the need for optimized transport mechanisms. TGA/DTG proved instrumental in quantifying these effects, supporting pozzolanic mechanisms for denser microstructures. Future work should explore injection systems and field trials to advance self-healing technologies, reducing infrastructure costs and promoting sustainability.

The second derivative TGA curve from Fig. 7 provides critical insights into the thermal stability and compositional complexity of the treated external section of concrete from UHE Assis Chateaubriand. The enhanced resolution reveals subtle transitions in moisture loss, hydration product decomposition, and carbonation effects, modified by the treatment, Acronal BS 796, and fumed nanosilica. The curve confirms a durable matrix with reduced porosity and stabilized hydration products, suitable for the harsh

hydroelectric environment. The treatment mitigates moisture ingress, while nanosilica and latex enhance C-S-H formation and matrix cohesion. The carbonation-related features highlight environmental exposure, distinguishing the external section from internal ones. Further quantitative analysis, such as peak deconvolution or comparison with untreated external sections, could refine the understanding of treatment effects. The curve underscores the concrete's optimized performance, supporting the use of these additives and treatments in infrastructure applications.

The second derivative TGA curve from Fig. 8 provides critical insights into the thermal stability and compositional complexity of the treated internal section of concrete from UHE Assis Chateaubriand. The enhanced resolution reveals subtle transitions in moisture loss and hydration product decomposition, modified by partial treatment, Acronal BS 796, and fumed nanosilica. The curve confirms a durable matrix with reduced porosity and robust hydration products, suitable for internal structural integrity in a hydroelectric environment. The treatment and additives enhance resilience, with minimal carbonation reflecting the internal section's protected nature. Further quantitative analysis, such as peak deconvolution or comparison with untreated internal sections, could refine understanding of treatment effects. The curve supports the concrete's optimized performance, validating the use of these additives and partial treatment in infrastructure applications.

Declarations

Acknowledgement

The authors gratefully acknowledge Elera Group for providing material for the research. We also thank Departamento de Ciência e Tecnologia Aeroespacial – DCTA (Brazil) through Aeronautics Institute of Technology – ITA (Brazil), George Mason University – GMU (USA) and Flowtest Engenharia e Pesquisa Ltda (Brazil) for their assistance on field tests and laboratory analysis.

Competing interests

This work was supported by Elera Group, Departamento de Ciência e Tecnologia Aeroespacial – DCTA (Brazil) through Aeronautics Institute of Technology – ITA (Brazil), George Mason University – GMU (USA) and Flowtest Engenharia e Pesquisa Ltda (Brazil).

Financial interests

The authors have no relevant financial or non-financial interests to disclose.

Funding declaration

The authors declare that this work was not supported by any research foundation or external funding.

Author Contributions

Dr. FBM: His contribution to the current study includes conceptualization, methodology, test preparation and full paper writing and editing. Dr. GSU: He has contributed to the field test, paper review and analysis of results. MGD: She has contributed to the investigation, methodology, test preparation and formal analysis of test results. BR: His contribution for the current study includes full test preparation, resource providing and analysis of results. Dr. LJ: He has contributed to test preparation and conduction and analysis of results. Dr. JAFFR: His contribution includes project administration, methodology, supervision in the field test and acquisitions. All authors have read and agreed to the published version of the manuscript.

References

1. Abid K, Gholami R, Choate P, Nagaratnam BH (2015) A review on cement degradation under CO2-rich environment of sequestration projects. J Nat Gas Sci Eng 27:1149–1157. https://doi.org/10.1016/j.jngse.2015.09.061
2. Araruna JCM (2021) Prevenção e recuperação de estruturas de concreto armado submetidas ao processo de corrosão da armadura. Trabalho de Conclusão de Curso, IFPB
3. Brown ME (2004) Introduction to Thermal Analysis, 2nd edn. Chapman and Hall, London
4. Campillo I, Dolado J, Porro A (2004) In: Bartos PJM, Hughes JJ, Trtik P, Zhu W (eds) Nanotechnology in Construction. Royal Society of Chemistry, pp 215–225. https://doi.org/10.1039/9781847551528
5. Chen W, Huang B, Yuan Y, Deng M (2020) Deterioration process of concrete exposed to internal sulfate attack. Materials 13(6):1336. https://doi.org/10.3390/ma13061336
6. Ghafari E, Arezoumandi M, Costa H, Júlio E (2015) Influence of nano-silica addition on durability of UHPC. Constr Build Mater 94:181–188. https://doi.org/10.1016/j.conbuildmat.2015.07.009
7. Inazumi S, Inazawa T, Soralump S, Saiki O, Matsumoto H (2017) Assessment of potassium silicate based surface penetration materials with low viscosity in the repair of concrete structures. Int J GEOMATE 12(29):163–170. http://dx.doi.org/10.21660/2017.29.160616
8. Kim JJ, Rahman MK, Al-Majed AA, Al-Zahrani MM, Taha MMR (2013) Nanosilica effects on composition and silicate polymerization in hardened cement paste cured under high temperature and pressure. Cem Concr Compos 43:78–85. https://doi.org/10.1016/j.cemconcomp.2013.07.002
9. Li LG, Zheng JY, Zhu J, Kwan AKH (2018) Combined usage of micro-silica and nano-silica in concrete: SP demand, cementing efficiencies and synergistic effect. Constr Build Mater 168:622–632. https://doi.org/10.1016/j.conbuildmat.2018.02.181
10. Lothenbach B, Le Saout G, Ben Haha M, Figi R, Wieland E (2012) Hydration of a low-alkali CEM III/B–SiO2 cement (LAC). Cem Concr Res 42:410–423. https://doi.org/10.1016/j.cemconres.2011.11.008
11. Mendonça FB, Urgessa GS, Domingues MG, Rocco BT, Junior LR, Rocco JAFF (2025) Retrofitting and waterproofing of aged concrete using electromigration of nanosilica: a case study. Braz J Chem Eng 42:295–304. https://doi.org/10.1007/s43153-023-00431-x

12. Meng B (1994) Calculation of moisture transport coefficients on the basis of relevant pore structure parameters. Mater Struct 27:125–134. https://doi.org/10.1007/BF02473025
13. Said AM, Zeidan MS, Bassuoni MT, Tian Y (2012) Properties of concrete incorporating nano-silica. Constr Build Mater 36:838–844. https://doi.org/10.1016/j.conbuildmat.2012.06.044
14. Shaikh FUA, Supit SWM, Sarker PK (2014) A study on the effect of nano silica on compressive strength of high-volume fly ash mortars and concretes. Mater Des 60:433–442. https://doi.org/10.1016/j.matdes.2014.04.025
15. Takagi EM, Junior AW (2014) Utilização de tecnologias de injeção para o aumento da durabilidade das estruturas de concreto armado. http://site.ibracon.org.br/. Accessed 18 Aug 2026
16. Villain G, Thiery M, Platret G (2007) Measurement methods of carbonation profiles in concrete: Thermogravimetry, chemical analysis and gammadensimetry. Cem Concr Res 37:1182–1192. https://doi.org/10.1016/j.cemconres.2007.04.015
17. XXVII ENCITA - Encontro de Iniciação Científica, ITA (2022)
18. Zhang Q, Ye G (2012) Dehydration kinetics of Portland cement paste at high temperature. J Therm Anal Calorim 110:153–158. https://doi.org/10.1007/s10973-012-2303-9
19. Zhu W, Bartos PJM, Porro A (2004) Application of nanotechnology in construction. Mat Struct 37:649–658. https://doi.org/10.1007/BF02483294

Figures

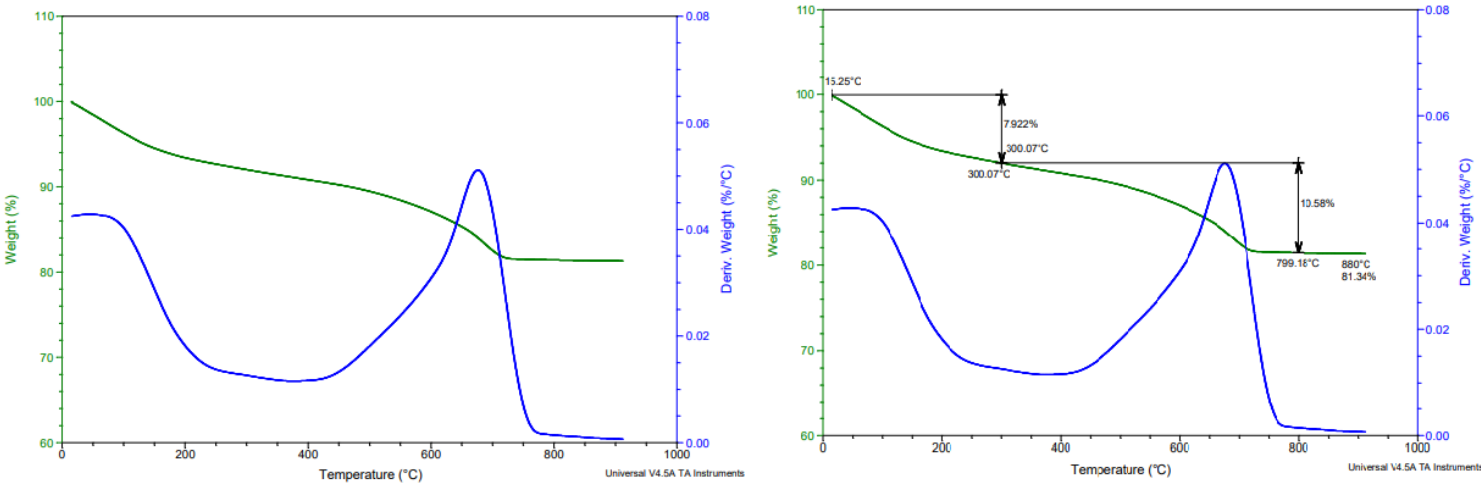


Figure 1

TGA/DTG curves of an untreated concrete sample from UHE Assis Chateaubriand (Acronal BS 796 + water + fumed nanosilica), at a heating rate of 10 °C/min

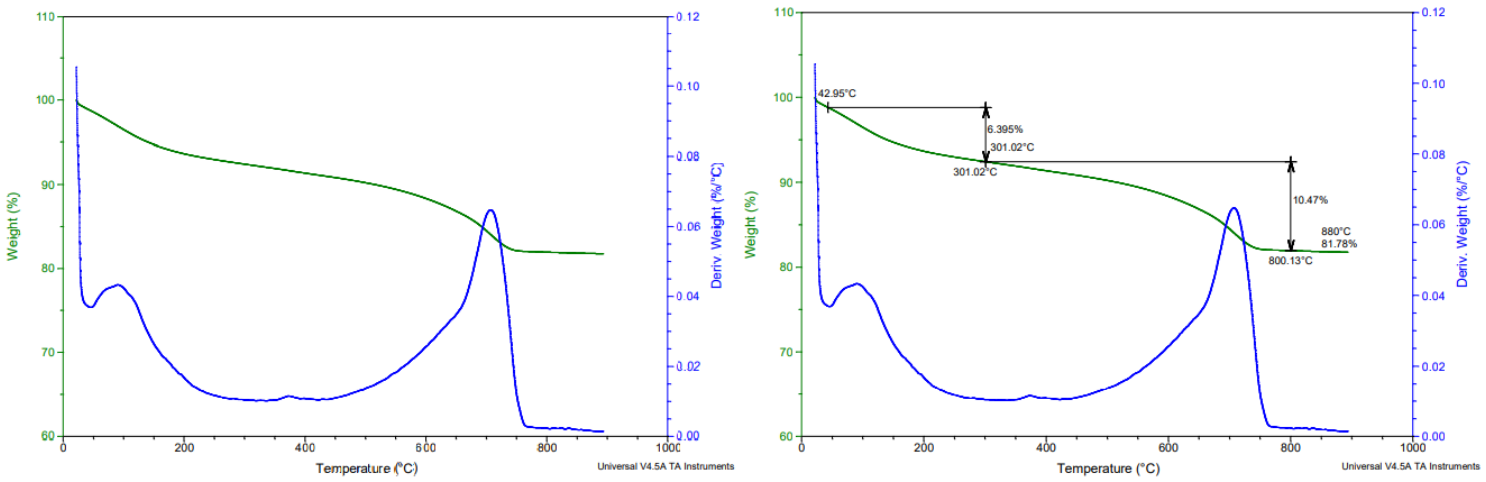


Figure 2

TGA/DTG curves of an untreated concrete sample from UHE Assis Chateaubriand (Acronal BS 796 + water + fumed nanosilica), at a heating rate of 20 °C/min

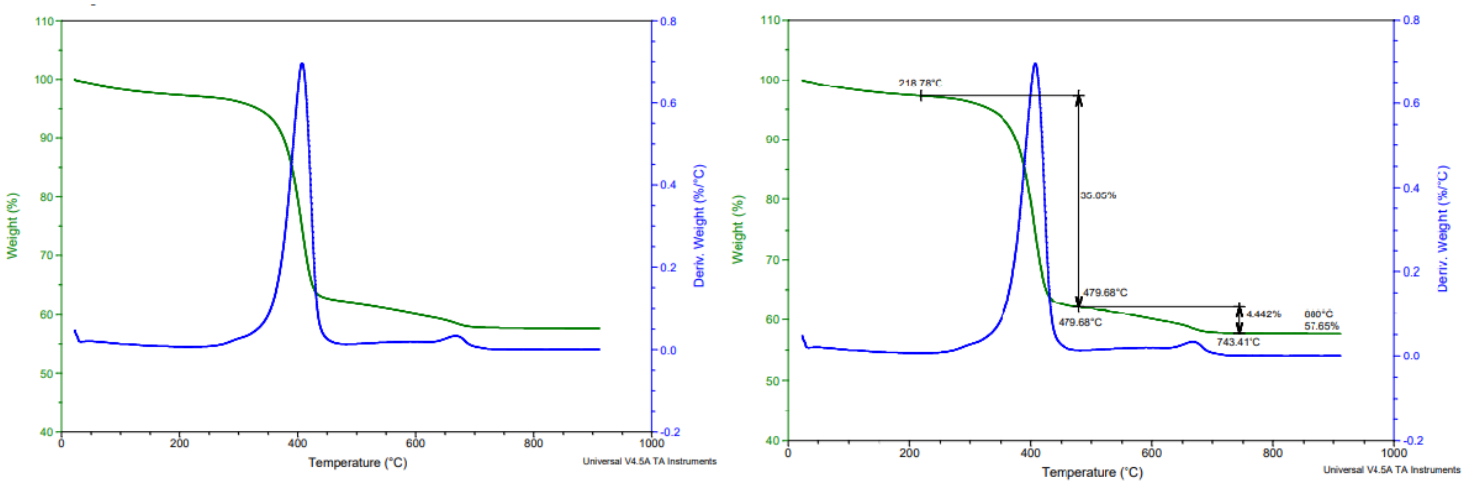


Figure 3

TGA/DTG curves of an external section of a treated concrete sample from UHE Assis Chateaubriand (Acronal BS 796 + water + fumed nanosilica), at a heating rate of 10 °C/min

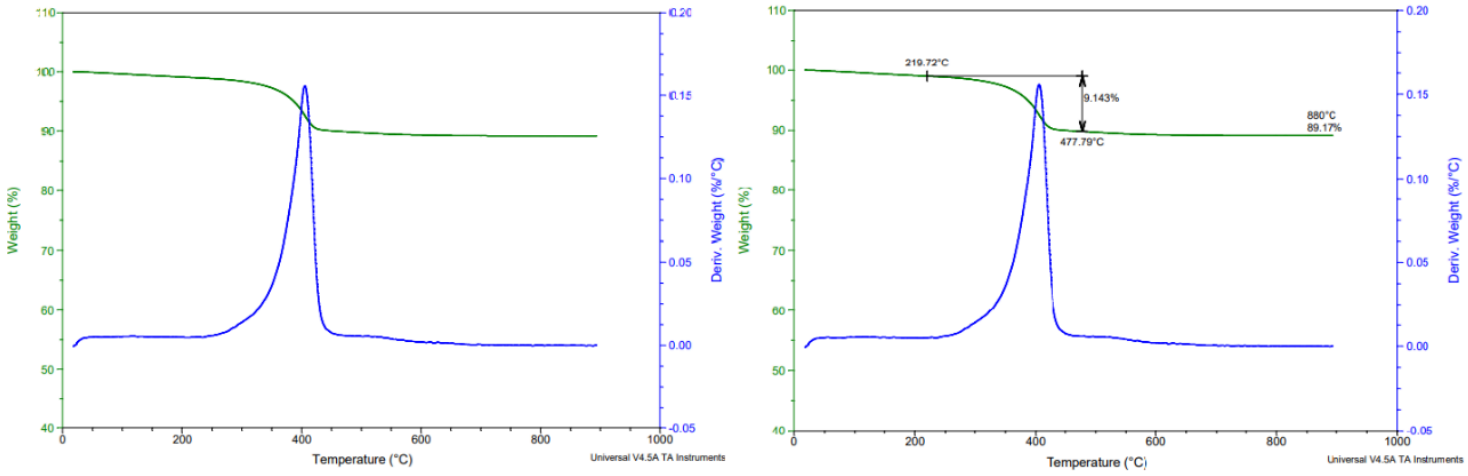


Figure 4

TGA/DTG curves of an external section of a treated concrete sample from UHE Assis Chateaubriand (Acronal BS 796 + water + fumed nanosilica), at a heating rate of 20 °C/min

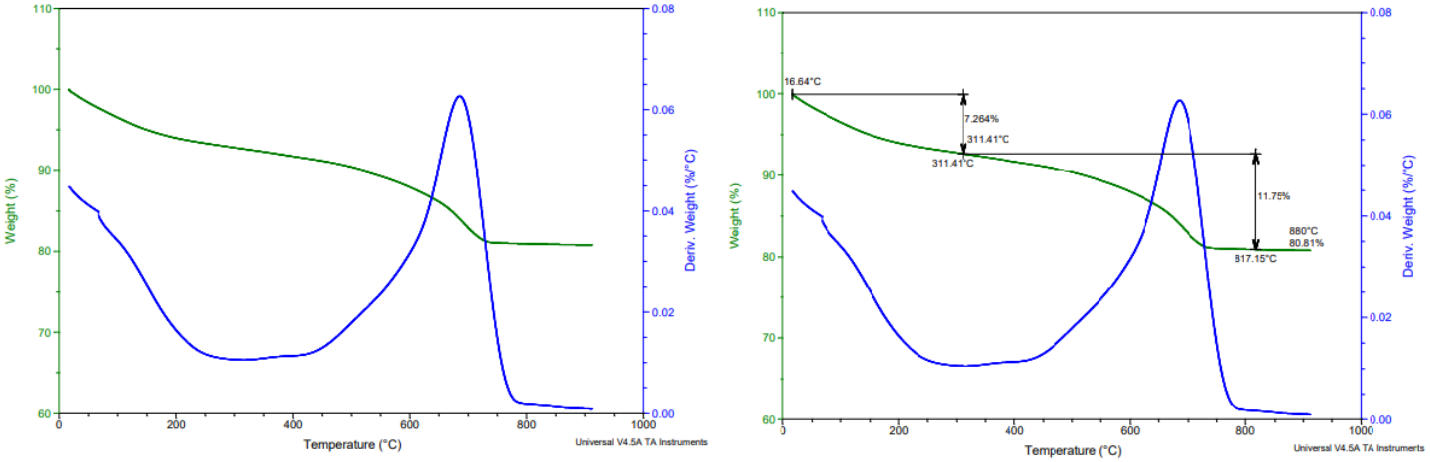


Figure 5

TGA/DTG curves of an internal section of a treated concrete sample from UHE Assis Chateaubriand (Acronal BS 796 + water + fumed nanosilica), at a heating rate of 10 °C/min

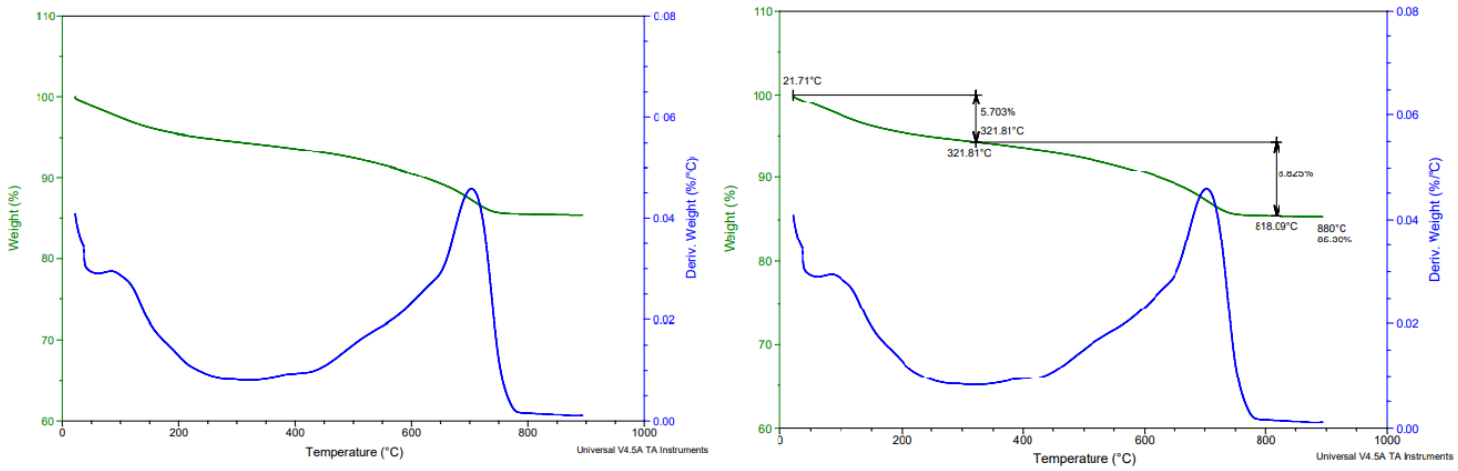


Figure 6

TGA/DTG curves of an internal section of a treated concrete sample from UHE Assis Chateaubriand (Acronal BS 796 + water + fumed nanosilica), at a heating rate of 20 °C/min

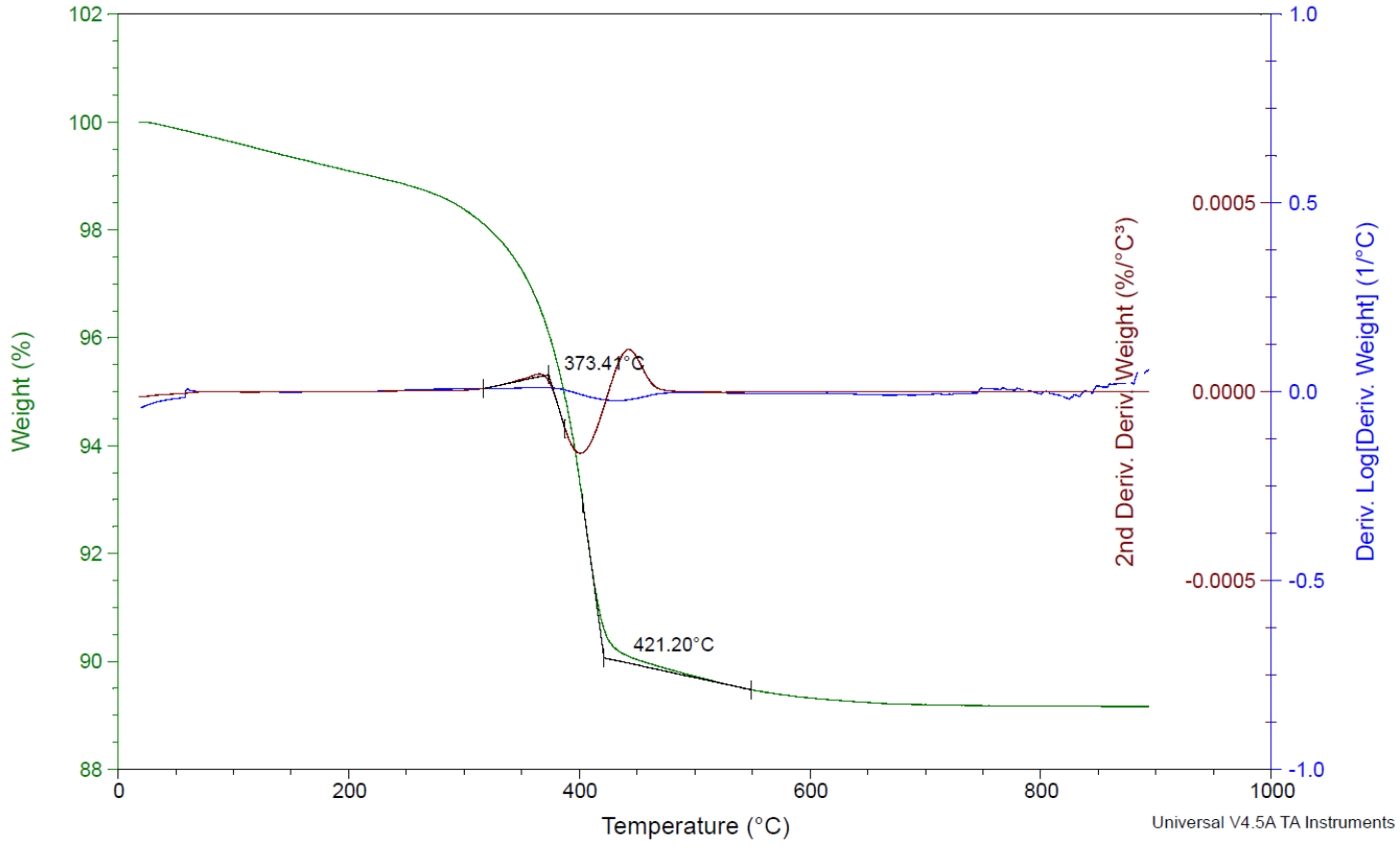


Figure 7

Second derivative TGA of the external section of a concrete sample from UHE Assis Chateaubriand

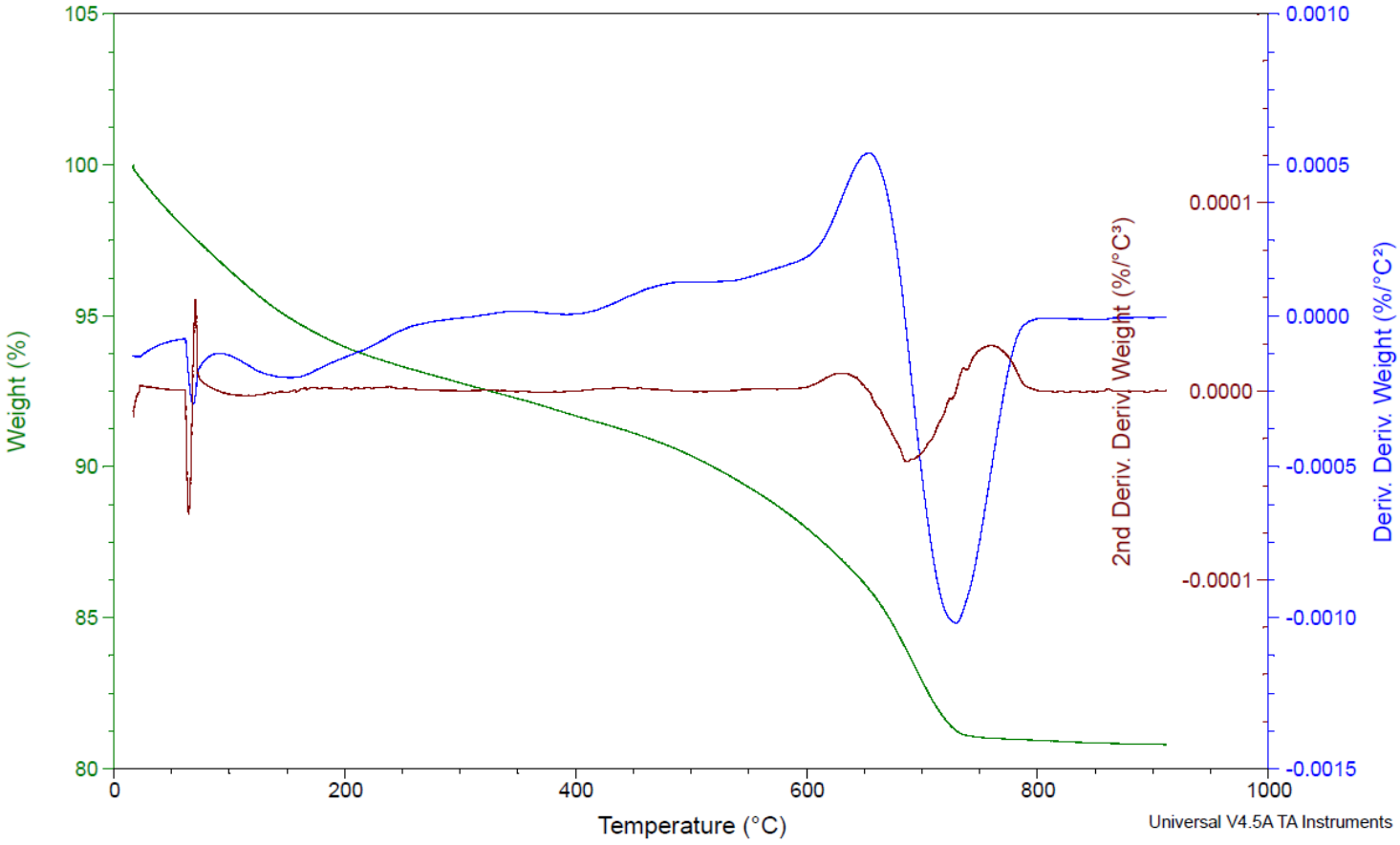


Figure 8

Second derivative TGA of the internal section of a concrete sample from UHE Assis Chateaubriand